An application of differential injection to fabricate functionally graded Ti- Nb alloys using DED-CLAD ® process

Catherine Schneider-Maunoury, Laurent Weiss, Olivier Perroud, David Joguet, Didier Boisselier, Pascal Laheurte

An application of differential injection to fabricate functionally graded Ti-Nb alloys using DED-CLAD® process

Catherine Schneider-Maunoury[a,b], Laurent Weiss[b,c], Olivier Perroud[b], David Joguet[d], Didier Boisselier[a], Pascal Laheurte[b,c,*]

[a] Irepa Laser, Parc d'Innovation, Pôle API, 67000 Illkirch-Graffenstaden, France
[b] Université de Lorraine, CNRS, Arts et Métiers ParisTech, LEM3, F-57000, Metz, France
[c] Laboratory of Excellence for Design of Alloy Metals for Low-mass Structures ('DAMAS' Labex), Université de Lorraine, France
[d] LERMPS, Université de Technologie de Belfort-Montbéliard, 90010 Belfort, France

ARTICLE INFO

Keywords:
Functionally graded material
Differential injection
Pre-alloyed powder
Titanium-niobium alloys
Additive manufacturing
Direct energy deposition

ABSTRACT

The aim of this paper is twofold: firstly, to compare the microstructural and the mechanical properties of Ti-44Nb samples manufactured pre-alloyed powder and differential injection, and secondly, to demonstrate the feasibility of the differential injection method included in the DED-CLAD® process, to manufacture functionally graded Ti-Nb alloys. Functionally graded materials (FGM) are promising new materials which are perfectly adapted to custom-made parts with various properties for specific applications. In FGMs, titanium and niobium ratios were modified in different steps to create the variation in alloy composition owing to a double-powder feeder. Mechanical analysis and SEM observations show the variation along the deposition depending on the chemical composition. Chemical analysis revealed the homogeneous repartition of the powder mixture as well as the nominal composition of each deposition. Mechanical tests showed a decrease of the microhardness with the increase of Nb content. The elastic modulus was found to be the lowest for Ti-40Nb.

1. Introduction

Construction Laser Additive Direct (CLAD®) is a metal additive manufacturing process. In this Directed Energy Deposition (DED) process, parts are manufactured layer-by-layer to obtain the required geometry. A large variety of materials could be manufactured for numerous applications in biomedical, aerospace, and automotive prototyping.

The versatility of this technology makes additive manufacturing interesting in particular for the manufacturing of Functionally Graded Materials (FGM). These new materials have been recently developed to combine the favorable physical and mechanical properties of two or more materials in one single part. The chemical composition is adjusted during the part manufacturing by varying the ratio of the different alloy powders melted and injected under a laser beam. The differential injection used to develop FGMs allows creating *in situ* specific chemical compositions that are currently unavailable in the market. By using numerous powder feeders, DED process allows the manufacturing of complex FGM parts. A variety of alloys based on two elements have already been studied. A non-exhaustive list includes: Ti-V (Collins et al., 2003), Ti-Mo (Collins et al., 2003; Ho et al., 1999; Zhang et al., 2015) or Ti-Ta (Nag et al., 2007) functionally graded in which the microstructure and mechanical properties evolved with the addition of the alloying elements were successfully manufactured without defect ; Ti6Al4V-Inconel 718 (Domack and Baughman, 2005) or Ti6Al4V-Inconel 625 (Pulugurtha, 2014) functionally graded in which cracks appeared due to the presence of Ti_2Ni, TiNi, $TiNi_3$, TiFe and $TiFe_2$ intermetallic compounds. Abioye et al. have also studied the functionally graded Ni-Ti alloy using CP Ti wire and Ni powder and have demonstrated the successful deposition of binary Ni-Ti layers on CP Ti layers (Abioye et al., 2015) ; SS304 L-Inconel 625 (Carroll et al., 2016) functionally graded where microhardness decreases and crack appear for 21% Inconel 625, while SS304 L-Invar 36 (Hofmann et al., 2014) was successfully manufactured without defect ; Ti6Al4V-TiC functionally graded in which the microstructure evolves with the modification of the chemical composition. Authors have demonstrated the great metallurgical bonding due the consecutive remelting (Mahamood and Akinlabi, 2015) ; Farayibi et al. have demonstrated the feasibility of functionally graded Ti6Al4V wire and WC powder for different powder feed rate of WC. The addition of WC improve hardness and wear resistance (Farayibi et al., 2013) ; Ti-Nb alloys were studied with fixe composition such as Ti-45Nb or Ti-27,5at.%Nb (Fischer et al., 2017;

* Corresponding author.
E-mail address: pascal.laheurte@univ-lorraine.fr (P. Laheurte).

Schwab et al., 2015) and with multiple gradients of composition from 0%, 5%, 10%, 15% and 20% of Nb (Han et al., 2015). Authors have highlighted the evolution of the microstructure, the mechanical properties and the cytocompatibility depending on the Nb content. They have demonstrated in particular the diminution of the Young modulus when Nb content increase from 10% to 20%. Wang et al. who have worked on different Nb content (from 0%, 15%, 25% and 45%) also have presented the presence of unmelted Nb into the deposition (Wang et al., 2017). Only one study about the functionally graded Ti-Nb alloy where the chemical composition varied from 0% to 100% Nb was referred in the literature. Despite the authors have presented the process parameters, the evolution of the chemical composition as well as the microhardness, no information are given about the crystallographic orientation, the mechanical properties such as the elastic modulus or the presence of unmelted particles (Cheung, 2015). Outside of this study, the maximum Nb content studied in the literature for binary Ti-Nb functionally graded alloys is 50% (Thoemmes et al., 2016).

The first part of the present work compares two techniques of part manufacturing with the DED-CLAD® process for a single chemical composition. The first one makes use of pre-alloyed powder, while the second one uses a differential injection allowing *in situ* mixing powder. This comparative study performed on Ti-44Nb alloy demonstrates the feasibility and the advantages of differential injection. The second part of this article focuses on the relationship between the microstructure and various properties of Ti-Nb functionally graded alloy in which the gradient of chemical composition was created by means of differential injection.

2. Experimental procedure

2.1. Materials

The materials used in the present work are pure titanium powder provided by TLS Technik, pure niobium and premixed Ti-44Nb wt% powders produced by H.C. Starck Tantalum and Niobium GmbH. The particle size distribution of both Ti and Ti-44Nb powders (Fig.1) ranged from 45 to 90 µm, while the pure Nb was below 63 µm to facilitate the melting of niobium (T_f = 2468 °C) with titanium (T_f = 1670 °C) powders. The three powders were spherical with some satellites and displayed a satisfactory flowability into the nozzle with respect to the process criterion. The materials were deposited onto a 100 mm × 100 mm × 8 mm Ti6Al4V substrate.

2.2. Laser processing

The parts were manufactured with a blown powder additive manufacturing process referred to as the DED-CLAD® process. The additive manufacture machine is equipped with a coaxial nozzle. A 2 kW laser diode was used, characterised by a 980 nm wavelength, a 600 µm fibre diameter and a focal point position at 12.5 mm. The energy distribution of the laser beam is top hat and the diameter of the beam at the focus point is 2.2 mm.

Due to the high affinity of Ti alloy with oxygen, manufacturing processes were carried out under argon gas. A gas purification system allows to maintained O_2 level below 20 ppm and H_2O level below 50 ppm.

Depending on the chemical composition of the deposit, the process parameters were adjusted. Laser power was adjusted in the range of 1800–2000 W, travel speed was set in the range of 2000–1500 mm/min, powder feed rate was adjusted in the range of 0–20 g/min and layer height step was set in the range of 0.5–0.8 mm.

In the case of pre-alloyed Ti44Nb, the powder is just sent into the coaxial nozzle before being deposited onto the substrate. Differential injection enables the manufacturing of *in situ* specific alloys such as binary Ti-44Nb as well as sample with FGM composition and thus a gradient of mechanical properties. For this purpose, differential injection was composed of two powder feeders, each one containing a different powder (Ti or Nb), alloying to control the variation in chemical composition. The powders are then injected into a homogenisation chamber where the powders are mixing before being injected into the coaxial nozzle and then deposited onto the baseplate.

2.3. Microstructure characterisation

The produced samples have been characterised by means of various techniques, such as optical microscope and scanning electron microscope to analyse the microstructures, electron backscatter diffraction to determine the crystallographic structure, X-ray diffraction to analyse the phase and tomography to quantify the unmelted particles. The different parameters have been described in our previous publication (Schneider-Maunoury et al., 2017).

2.4. Mechanical tests

Microhardness analyses were performed using a Buehler machine with an applied force of 500 g and a dwell time of 15 s. Three lines of measurement with a 0.75 mm of line interval were performed starting from the substrate up to the top of the sample. Approximately 5 indents every 0.35 mm along the building direction were performed on gradient of composition (Fig.2).

Uniaxial tensile specimens with bone shape were cut using a water jet process to avoid microstructural modification. Tensile tests were carried out by means of a universal tensile test machine, Zwick Roell, and data were processed with Test Xpert II. Three types of sample have been particularly manufactured for the tensile tests:

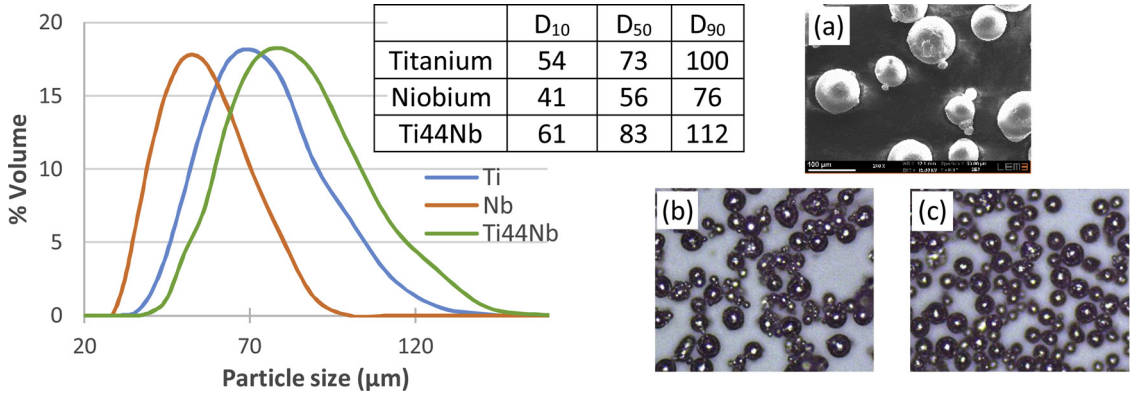

	D_{10}	D_{50}	D_{90}
Titanium	54	73	100
Niobium	41	56	76
Ti44Nb	61	83	112

Fig. 1. Particles size distribution for Ti and Nb powders, and Ti44Nb pre-alloyed powder. SEM and optical micrograph showing the spherical (a) Ti44Nb, (b) Ti and (c) Nb powders.

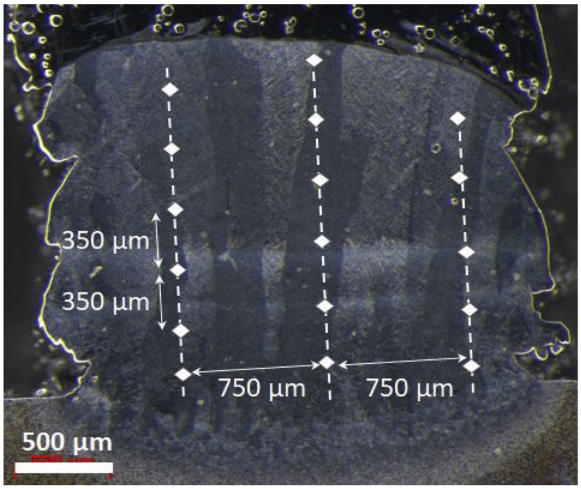

Fig. 2. Microhardness measurements along the cross section of the sample.

- Two samples with single composition (Ti-44Nb) to compare two manufacturing techniques: pre-alloyed powder and differential injection,
- One sample with five gradients of composition (from 5% Nb, 10% Nb, 40% Nb, 70% Nb and 100% Nb),
- Four samples with different percentage of niobium to illustrate the FGM sample behaviour (4 samples composed of 5% Nb, 10% Nb, 40% Nb and 70% Nb).

The laser scanning strategy as well as the tensile specimens along the building direction of the sample can be seen in Fig.3. Four tensile specimens were taken from each build.

3. Results and discussion

3.1. Comparison between pre-alloyed powder and differential injection

This section compares the metallurgical and mechanical properties of additively manufactured Ti-44Nb alloy parts prepared from pre-alloyed powder and by means of differential injection with melting of in-situ pure titanium and pure niobium powders.

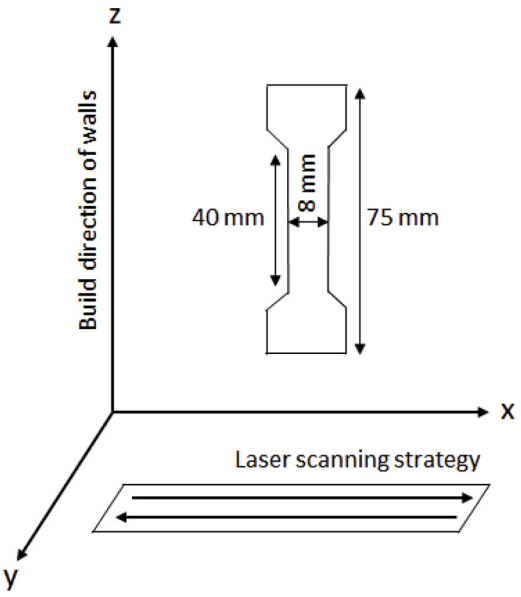

Fig. 3. Dimension and orientation of tensile specimen cut in the sample depending on the laser scanning strategy.

3.1.1. Distribution of chemical elements

Chemical analyses were performed for each sample to check the nominal composition of the deposited material as well as the homogenous distribution of different chemical elements. Fig. 4a and b show the measurements carried out across three tracks in height (distance of 2.5 mm). Fig. 4c shows the nominal composition of Ti-44Nb using pre-alloyed powder and Ti-38Nb using differential injection. The pre-alloyed powder has the expected composition announced by the powder manufacturer while the sample manufactured by differential injection system presents a nominal composition below the expected amount of 44% of niobium. The 6% difference in the chemical composition in sample manufactured with differential injection can be explained by the presence of a very small part of unmelted Nb particle or by an underestimation of the programmed composition.

The presence of some unmelted particles observed by MEB is due to the high difference in melting temperature between titanium and niobium and the insufficient energy density to fully melt the niobium powder. Chlebus et al., who have investigated the manufacturing of titanium alloy with rhenium addition by the SLM process, have demonstrated that the conventional process parameters commonly used for titanium powder are not sufficient to melt Re particles having higher melting point (Chlebus et al., 2014). Even though high-density alloys were obtained using an energy density 4.5 times larger, the Re particles were still detected. The authors have suggested the use of higher energy density and sieved Re powder to completely dissolve Re in Ti. In our study, although unmelted Nb particles were present in our samples, in both cases a homogeneous distribution of titanium and niobium into the deposited sample could be achieved.

3.1.2. Phases and microstructures analyses

The crystallographic phase of each sample was identified by X-ray diffraction (Cu Kα X-ray) and the results are summarized in Fig. 5. The Ti6Al4V plate consisted of α-phase (hexagonal structure) with a small volume fraction of β-phase (cubic centred structure), of around 8%. The β-phase is dominant during the high temperature deposition of both pre-alloyed powder and differential injection. Elmay et al. who worked on a Ti-38 wt.%Nb and Ti-40.5 wt.%Nb (Elmay et al., 2013) have highlighted the presence of α" phase (orthorhombic structure) dominant in Ti-38%Nb, while the Ti-40.5%Nb alloy was fully composed by the β-phase stable at room temperature. The cooling velocity which is higher for the cold crucible levitation melting process (Elmay et al., 2013) than that of direct metal deposition, could explain the β-phase dominance in Ti-44Nb in the present study. The cooling velocity also depends on the build structure. But, in this study, the small thickness of the sample lead to a rapid cooling.

The microstructures of both materials prepared by pre-alloyed powdered and the differential injected are similar, as shown by Fig.6. However, it should be noted that some unmelted particles are visible in the sample manufactured by the differential injection deposition. These unmelted particles are spherical with a diameter between 5–40 µm and are identify as niobium. A very small dilution around 10 µm has been measured around the unmelted particle.

The EBSD maps showing the grain morphology of the samples prepared by the two different approaches are presented in Fig.7. In both cases, β-grains have equiaxed morphology without specific crystallographic orientation and the grain size distributions was similar (around Ø30 µm by differential injection and around Ø35 µm by pre-alloyed powder). The initial indexation rate of the map in Fig.7a was about 78% and Fig.7b was about 75%. Because of the presence of coarse β-grains, noise reduction has been performed to get indexation rate of 100%.

3.1.3. Mechanical properties

Microhardness measurements were performed using a Vickers microhardness indenter. The microhardness of the Ti-44Nb alloy using pre-alloyed powder and differential injection were 212 ± 5 HV and

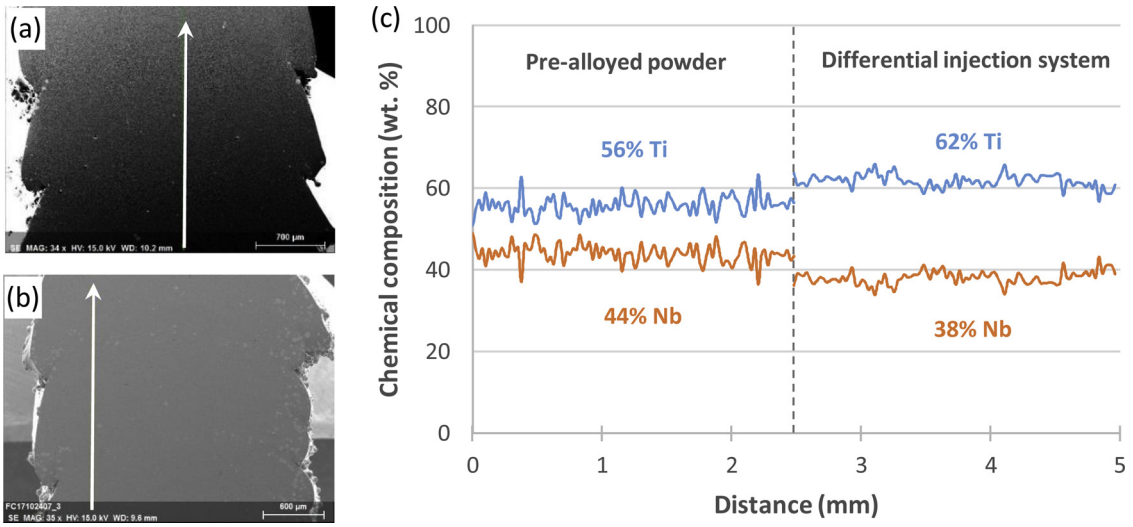

Fig. 4. Line scan measurements across the deposition using (a) pre-alloyed powder and (b) differential injection; (c) Variation in the chemical composition of the deposited materials by the two techniques.

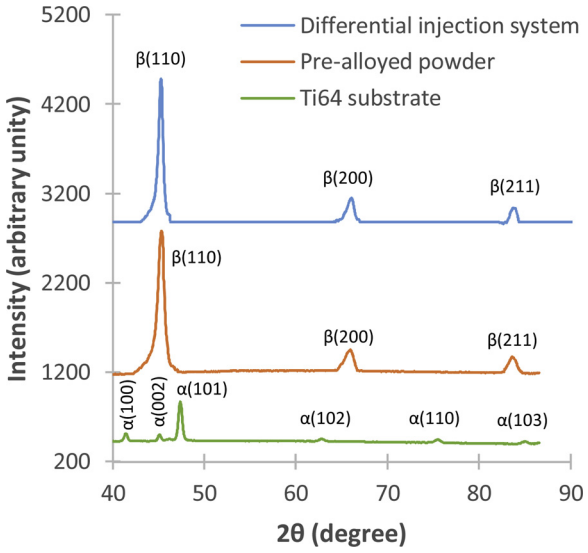

Fig. 5. X-ray diffraction of samples manufactured by pre-alloyed powder and differential injection.

228 ± 14 HV, respectively. These results are quite similar in both cases and are in accordance with value reported in the literature, i.e., ˜210 HV for Ti-40Nb (as-melt alloy) (Thoemmes et al., 2016).

The mechanical properties of the samples, mainly the Young's Modulus, have been determined by means of tensile tests. The tests were carried out using a cross speed of 1 mm/min. The results shown in Fig.8 and Table 1 were obtained from an average of four experiments. The value of the elastic modulus for pre-alloyed powder and differential injection were 60 ± 4 GPa and 69 ± 33 GPa, respectively. This elastic modulus is significantly lower than that of pure titanium (120 GPa) and close to that of cortical bone (10–30 GPa). Moreover, the ultimate tensile strength stress of both samples were 700 ± 22 MPa for the pre-alloyed powder and 723 ± 26 MPa for the differential injection. The main difference between both methods is the elongation at rupture. This was observed to be 2 ± 1% for alloys prepared pre-alloyed powder and 23 ± 3% for differential injection system.

As the sample were carried out under argon gas, the significant difference in the elongation at rupture observed in tensile tests can be attributed to the high oxygen concentration initially contained into the pre-alloyed powder that remained into the deposition due to the absence of desorption, as indicated in Table 2 and in accordance with the results from Kim et al. (Kim et al., 2005). These analyses suggest the absence of contamination during manufacturing. This result is in agreement with those of Wei et al. who have demonstrated that the interstitial strengthening effect was responsible for the decrease in elongation with increasing the oxygen content (Wei et al., 2011).

3.2. Functionally graded titanium-niobium alloy obtained by differential injection

The DED process requires powders with chemical composition corresponding to those of the expected alloys. However, some chemical compositions are rare, expensive or unavailable in the market. For these

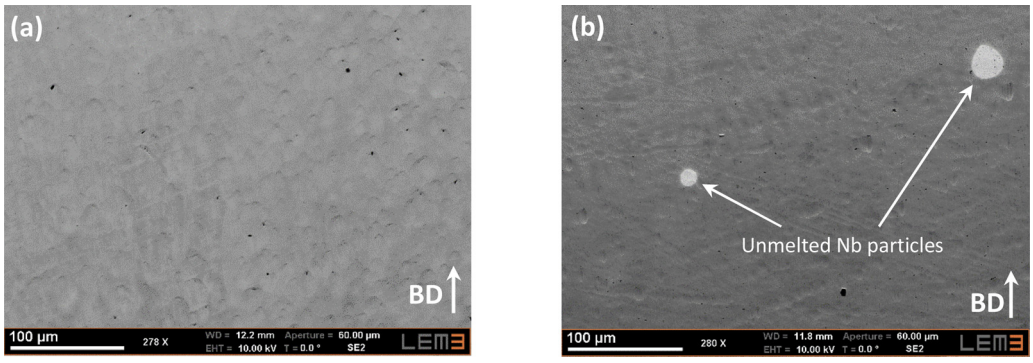

Fig. 6. Microstructure of (a) sample manufactured with pre-alloyed powder and (b) sample manufactured with differential injection.

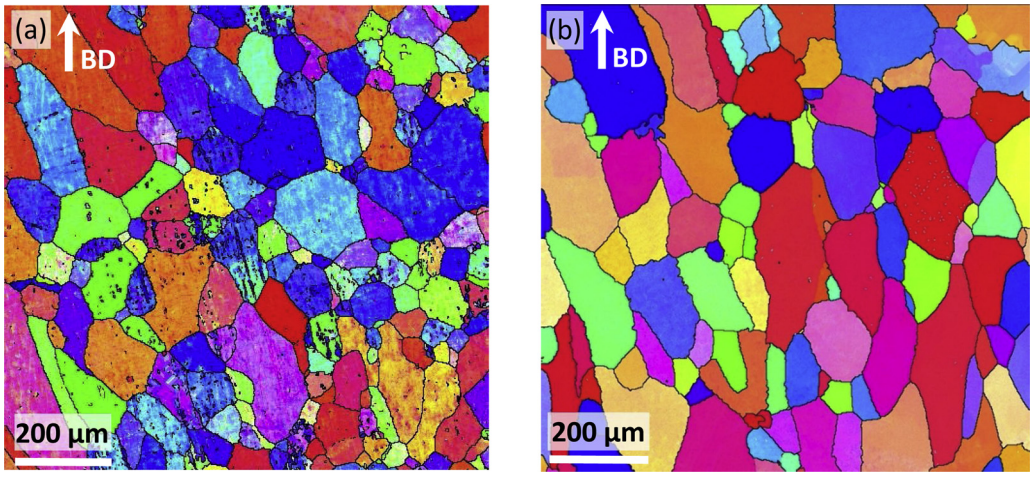

Fig. 7. Crystallographic orientation maps of (a) sample manufactured with pre-alloyed powder and (b) sample manufactured with differential injection.

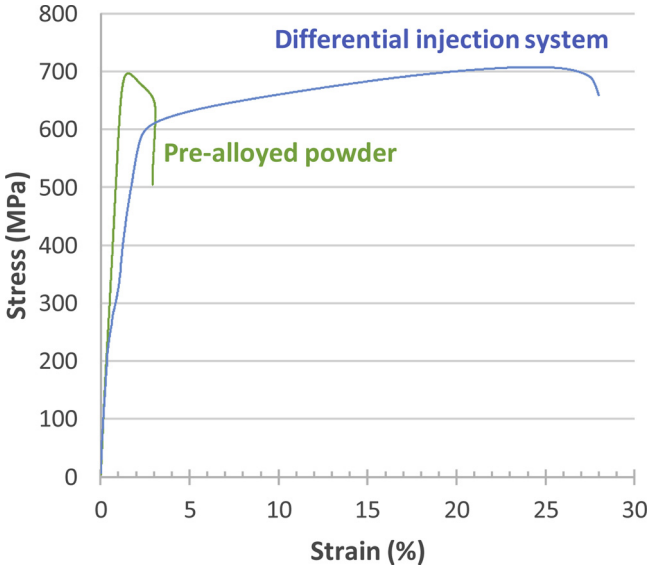

Fig. 8. Stress-strain curves for sample manufactured by using pre-alloyed powder and differential injection.

Table 1
Mechanical properties of Ti44Nb alloy manufactured by using pre-alloyed powder and differential injection.

	$\sigma_{0,2}$ (MPa)	σ_m (MPa)	A%	E (GPa)
Pre-alloyed	626 ± 34	700 ± 22	2 ± 1	60 ± 4
Differential injection	568 ± 57	723 ± 26	23 ± 3	69 ± 33

Table 2
Oxygen amounts in pure Ti and pure Nb powders, in Ti44Nb pre-alloyed powder, and after deposition by using pre-alloyed powder and differential injection.

	Powders	After deposition
Ti44Nb	2500 ppm	2430 ppm
Ti	1400 ppm	1270 ppm
Nb	520 ppm	

reasons, the differential injection presents a real advantage to create special *in situ* alloys with variation in composition. Moreover, the opportunity to create the chemical composition during manufacturing could open new opportunities to obtain custom-made parts for a wide range of applications such as aerospace (Domack and Baughman, 2005; Qian and Dutta, 2003) and biomedical (Bandyopadhyay et al., 2009; Watari et al., 1997).

Accordingly, two samples were manufactured using differential injection to create alloys with a gradient of chemical composition. In sample n°1, the Nb content varied from 5% Nb, 10% Nb, 40% Nb, 70% Nb, 100% Nb, and in sample n°2 the Nb content varied from 0% Nb, 25% Nb, 50% Nb, 75% Nb, 100% Nb. These compositions have been chosen in case of sample n° 1 to compare the microstructural and mechanical properties with the binary alloys ever studied in the literature (Lee et al., 2002; Thoemmes et al., 2016; Wang et al., 2017) and in the case of sample n° 2 to compare with another alloy such as Ti64-Mo (Schneider-Maunoury et al., 2017) and thus observe the behaviour difference depending on the alloy element. Each sample consisted of a single-track width sample with five gradients of the chemical composition with at least four layers deposited in order not to suppress the dilution effect between adjacent layers.

3.2.1. *Homogeneity and unmelted particles*

Chemical analyses were performed for each deposition layer with the aim of comparing the nominal composition with the programmed one. Results obtained for the two samples are summarized in Fig.9. The five gradients have the expected composition, with an uncertainly of ± 1%. In the case of sample n°2, i.e. the sample with an increase or a decrease of 25% between each gradient, peaks are observed in the gradient composed by 75% Nb. This is explained by the fact that measurement is performed across unmelted niobium with a strong dilution affect around the particle. Moreover, it can be observed that the compositions of gradients comprised from 25% to 75% of Nb present fluctuations. These fluctuations could be explained by the formation of a dendritic substructure. Fallah et al. have obtained similar results on Ti-45Nb alloy characterised with Ti-rich fine dendrites and coarse dendrites rich in Nb (Fallah et al., 2010). In additive manufacturing with differential injection, similar microstructural features were also observed in functionally graded titanium-molybdenum alloys (Schneider-Maunoury et al., 2017).

The homogeneous distribution of titanium and niobium elements into the deposited graded layers were verified and validated by the EDS analyses. However, the results revealed the presence of a few unmelted Nb particles, which seem to be localized at the interfaces between two deposited tracks, regardless of the chemical composition. A tomography analysis performed on sample n°1 (Fig.10) confirmed these observations for the alloy containing up to 40% Nb.

Tomography tests performed on sample n°1 enabled the quantification of the number of unmelted Nb particles. During tomography test, a first work on the section view consists to remove the side effect as well

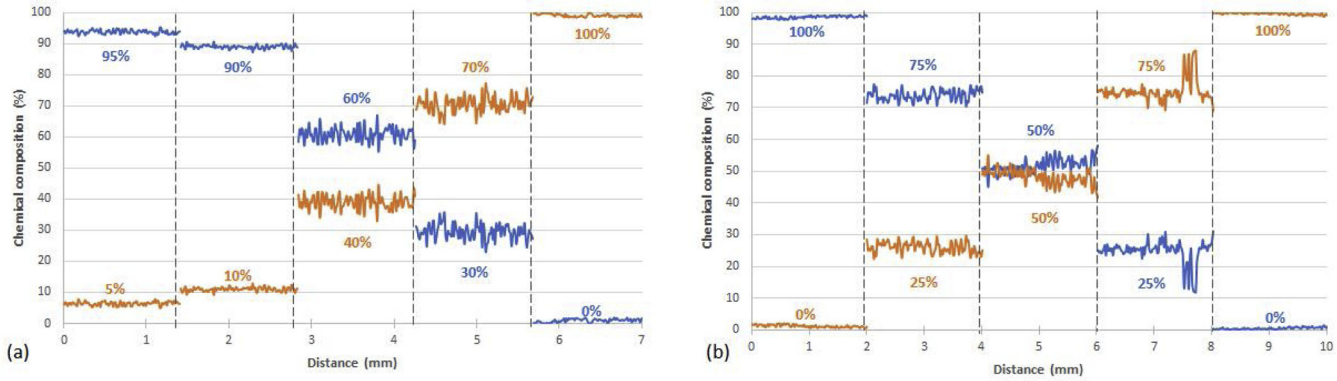

Fig. 9. Chemical composition variation across the deposited material (a) sample n°1 and (b) sample n°2.

as artefact such as ring. After this post treatment, the volume of the sample is rebuilt in 3D. Some filters were applied for the segmentation of grey levels.

Fig. 11 represents the number of unmelted Nb particles depending on the wt.% Nb. It can be observed that at most 1% of unmelted particles are present into the deposited material. It should be noticed that in these analyses, data obtained by tomography were treated and individual point smaller than a given size were deleted (voxel size 13.05 µm). Thus points visible on the two last gradients in Fig. 10a and b were not taken into account. This also explains the absence of unmelted particles for Nb content above 70% in Fig. 11. The same conclusions could be made for sample n°2.

These results have been compared with the quantification of unmelted particles obtained by optical microscope (after metallurgical preparation, the full area of each gradient, i.e. around 2.5 mm wide and 2 mm height, has been observed and unmelted particles have been measured with AxioVision software). This latter technique highlights an increase in the number of unmelted Nb particles as the Nb content increased in the deposition (Fig. 11). However, measurements obtained by optical microscopy are limited to a 2D analysis. This means that in another cross-section, a larger or smaller number of unmelted particles could be observed. Moreover, the measurement could take into consideration partial dilution at the periphery of the particles. Nevertheless, the number of unmelted particles detected by optical microscope is still lower than 4%.

The quantification of the number of unmelted Nb particles

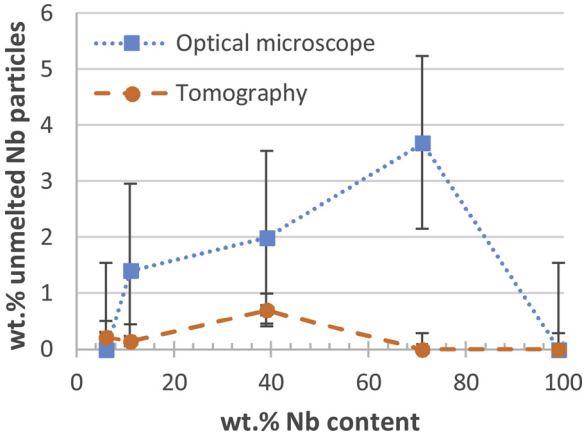

Fig. 11. Quantification of unmelted Nb particles by tomography and optical microscopy.

highlights the importance of performing 2D and 3D analysis in additive manufacturing studies. Indeed, as tomography is based on the material absorption difference, it is not adapted for analysing layers composed of 100% Nb. Moreover, as multiple unmelted particles have been observed on the outer surface of the sample and due to the well-known side effect in tomography, it is necessary to perform optical microscopy analyses, both techniques providing complementary information. Despite the

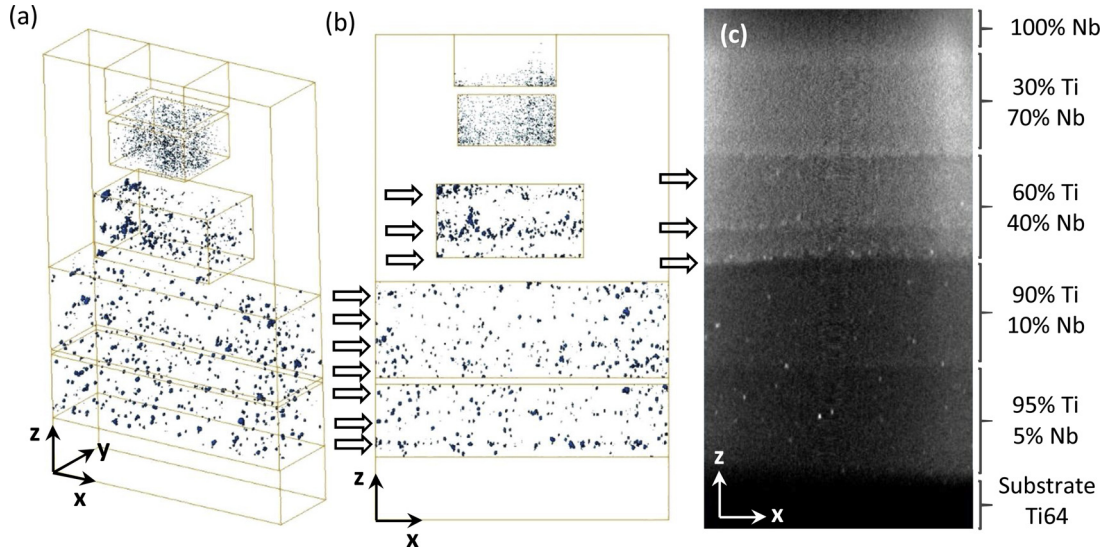

Fig. 10. Distribution of unmelted Nb particles along the functionally graded Ti-Nb sample. (a–b) 3D view and xz plane, respectively. (c) Reconstructed view after tomographical acquisition (unmelted particles in white; matrix in shades of grey).

measurement error associated with both techniques, the amount of unmelted Nb particles was substantially lower than that of unmelted particles present in other binary alloys such as Ti-26Nb (at.%) (Fischer et al., 2016), or the recently reported functionally graded Ti64-Mo (Schneider-Maunoury et al., 2017). Some authors have demonstrated that the number of unmelted particles can be significantly reduced by increasing the energy density (Chlebus et al., 2014; Fischer et al., 2016). The higher density of niobium (8.57 $g.cm^{-3}$) compared to that of titanium (4.51 $g.cm^{-3}$) can lead to Nb elements to sinking to the bottom of the melt pool before solidification of the melt pool. This hypothesis can explain the presence of unmelted particles present at the interface between two layers.

Three hypotheses could be made about the origin of unmelted particles. Firstly, the flying time of particle could be insufficient to allow the homogenous temperature of particle and thus the fusion before their arrival in the melt pool. Secondly, optical properties of the powders such as the absorption coefficient and the emissivity at solid or liquid state, could influence the fusion of the particle. As titanium achieves its melting temperature before niobium (T_{f_Ti} = 1660 °C and T_{f_Nb} = 2470 °C), its emissivity at liquid state drop before the niobium one. Thus, it seems that titanium absorbs more energy and there is not enough energy for the fusion of niobium. Thirdly, the formation of plume composed by ultra-fines titanium particles due to the titanium vaporization lead to a screen effect of energy on the niobium particles (DebRoy et al., 1991; Greses et al., 2004; Matsunawa and Ohnawa, 1991).

3.2.2. *Phases and microstructures evolution*

Using X-ray diffraction patterns (Fig. 12a), the phases present in the material manufactured with variation in chemical composition (sample n°2) were identified. The Ti6Al4V substrate displayed a typical α-phase corresponding to the hexagonal structure. The Ti6Al4V deposition consisted of a hexagonal α'-phase formed by the rapid cooling of columnar beta grains, as explained by Weiss et al. (Weiss et al., 2016). When Nb content is ramped up to 25%, the high temperature bcc β-phase was entirely retained. Lee et al. have highlighted the presence of the α"-phase, particularly dominant for composition between 17.5% and 25% Nb (Lee et al., 2002). This phase has also been observed in other titanium alloys. Increasing the Nb content up to 27.5% led to a small amount of β-phase. In contrast, for Nb contents larger than 30%, the α"-phase does not form and the β-phase becomes the major phase. This is in accordance with the results obtained in the present study, although α"-phase has not been detected. It is believed that the successive remelting of the sample is likely to create a reversible transformation α" →β which could explain why the α"-phase is not detected in the X-ray diffractograms. X-ray diffraction results also prove that niobium operates as beta-stabilizer element, thus avoiding the martensitic transformation during cooling.

Values of the lattice parameters calculated using X-ray diffraction patterns are summarized in Fig. 12b. The value of the Ti6Al4V lattice parameter was found to be 0,3196 nm. Parts of the graded alloyed preparing with 25%–100% Nb showed a lattice parameter around 0,327 nm. Using X-ray diffraction, it has been demonstrated that the Nb content has no specific influence on the lattice parameters, which is in accordance with the results of Yao et al. (Yao et al., 2007). This appears to be sound since the metallic radius of Ti (147 pm) and Nb (146 pm) are almost identical and the atoms are replaced in substitution.

The microstructural evolution depended on the chemical composition of the deposited layers. The first layers rich in Ti consisted of martensitic microstructure. When the Nb content was increased between 25% and 75%, a dendritic substructure was observed in the β-grains, revealed by the Ti-rich phases (dark area) and phases rich in Nb (light area) shown in Fig.13. The dendritic microstructure was observed by Fallah et al. in their work on the laser cladding of Ti-45Nb. This substructure was explained by the cooling rate during solidification (Fallah et al., 2010). The last 100% Nb deposition presented coarse and

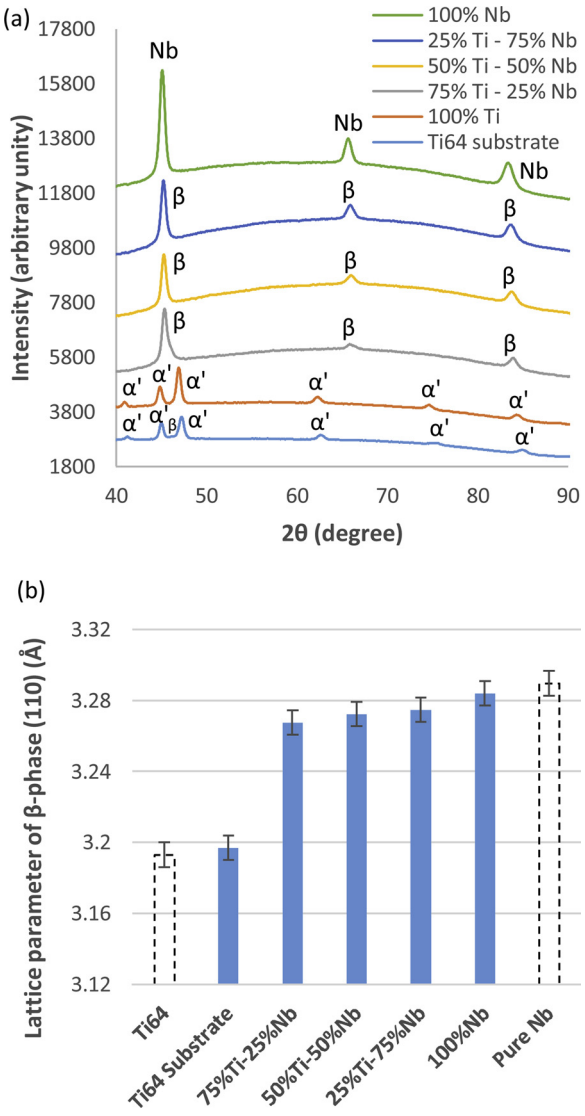

Fig. 12. (a) X-ray diffraction patterns and (b) lattice parameters of functionally graded titanium-niobium sample in sample n°2 manufactured by differential injection.

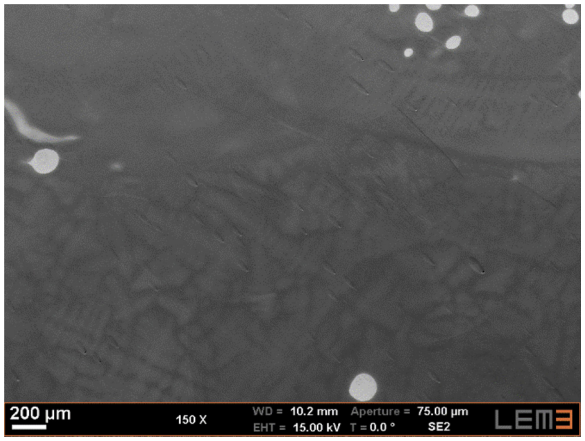

Fig. 13. Dendritic substructure of 75% Ti - 25% Nb deposition.

elongated β-grains.

The chemical composition variation also led to crystallographic modification, as shown in Fig. 14(b–f). The first 100% Ti deposited

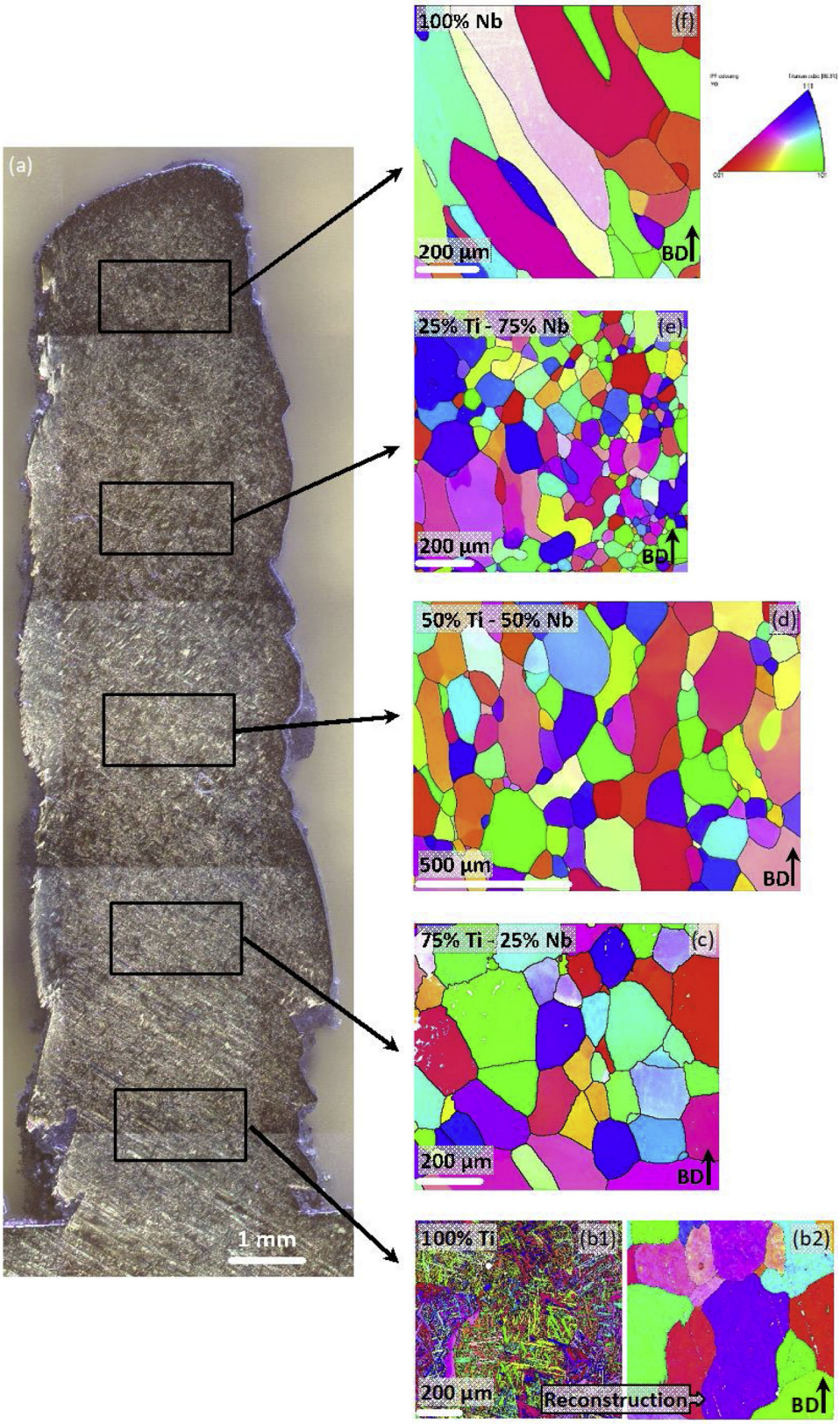

Fig. 14. (a) Optical macrograph of sample n°2. (b–f) Crystallographic orientation of Ti-Nb alloys with the Nb content. (b1, b2) Measured before and after β-phase reconstruction.

material presented fine martensitic needles (Fig. 14b1). Fig. 14b2 shows the EBSD reconstructed map before martensitic transformation, i.e., the β-phase grains (reconstruction with Merengue2 software (Germain et al., 2012)). Unlike the 100% Ti6Al4V deposition, the pure titanium deposition presented coarse β-grains without marked crystallographic orientation. From 25%–75% Nb, grains were equiaxed without specific crystallographic orientation. Moreover, a slight difference in grain size could be observed with a small increase between

Table 3
Mechanical properties of functionally graded Ti-Nb alloy from tensile tests.

	$\sigma_{0,2}$ (MPa)	σ_m (MPa)	A%	E (GPa)
95% Ti - 5% Nb	452 ± 31	510 ± 23	12 ± 5	99 ± 12
90% Ti - 10% Nb	543 ± 37	630 ± 22	11 ± 7	76 ± 10
60% Ti - 40% Nb	470 ± 31	513 ± 19	11 ± 5	58 ± 8
30% Ti - 70% Nb	423 ± 9	480 ± 4	10 ± 4	70 ± 7
Sample with gradient of composition	–	383 ± 16	–	76 ± 2

25%–50% Nb (from around Ø 64 µm to Ø 90 µm, respectively) followed by a small decrease between 50%–75% Nb (around Ø 52 µm for 75% Nb). The final layer composed by 100% Nb presented coarse columnar β-grains (540–1160 µm long and 90–125 µm large) tilted of about 60° and without specific crystallographic orientation. The grain tilt observed in the last gradient could be explained by a defocusing of the powder jet, which leads to a tilted manufacturing of deposited layers, and thus to a grain growth perpendicularly to the interface.

3.2.3. *Modification of the mechanical properties*

Based on the chemical composition of sample n°1, four samples were manufactured with a single chemical composition while one sample was manufactured with a gradient of composition. Because the energy density was insufficient to manufacture the part of the sample with 100% Nb with correct metallurgical bonding, no mechanical test was performed for this chemical composition. Table 3 summarizes the mechanical properties for each chemical composition. The results were an average from four experiments per build. The stress-strain curves of Ti(5%–70%)Nb can be seen in Fig. 15.

Our results indicated that an increase in Nb content from 5% to 40% led to a marked decrease in the elastic modulus from 99 GPa to 58 GPa, respectively. For higher Nb content, Young's modulus increased again to 70 GPa. As explained by Chlebus et al., the Young's modulus of the β-phase is the lowest among all phases of titanium alloy (Chlebus et al., 2011). The addition of Nb leads to the appearance and stabilization of the β-phase, and therefore reduces the elastic modulus. However, further increases in the Nb content led to a large amount of the unmelted Nb particles responsible for the increase in the elastic modulus (Wang et al., 2017). These results demonstrate the high potential for the biomedical application regarding the results of titanium-niobium alloy with Nb content around 40%. These binary alloys provide a low elastic modulus with values close to that of cortical bone favorable for the reduction in the stress-shielding effect. Kim et al. have observed a decrease of the yield stress when Nb content increased from 20 at.% to 26 at.% due to the reorientation of martensite variants (Kim et al., 2004).

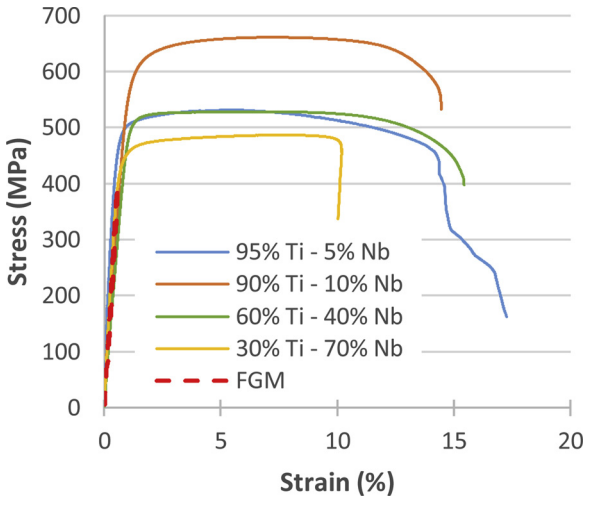

Fig. 15. Stress-strain curves of binary Ti-Nb alloy and functionally graded Ti-Nb alloy.

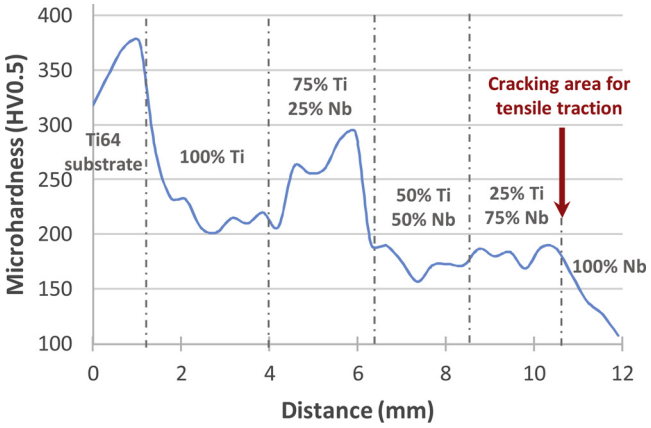

Fig. 16. Microhardness variation along the functionally graded Ti-Nb alloy. Tests performed on sample n°2.

During tensile tests in the functionally graded tensile specimens, crack formations were observed at the interface between 70% and 100% Nb (Fig. 15) and were found to appear in the elastic domain. This show the very brittle behaviour at this interface which is due to the insufficient energy density to fully melt the pure niobium and to create a good metallurgical bonding.

Microhardness tests performed from the substrate to the top of the sample are presented in Fig.16. The Ti6Al4V substrate showed a microhardness of ˜350 HV, in agreement with the values found in the literature (Kottcamp and Langer, 1992). Pure titanium and pure niobium deposits have a microhardness of around 215 ± 12 HV and 124 ± 15 HV (Syre, 1976), respectively. When niobium content was in the range of 0–25%, the microhardness increased to 258 ± 36 HV. This increase in the microhardness was explained by some authors by the presence of a small fraction of ω-phase (Lee et al., 2002; Thoemmes et al., 2016). As the DED-CLAD® process consists in manufacturing parts layer by layer, each layer experiences remelting. This leads to tempering, which could promote the formation of the ω-phase and explain the increase in the microhardness. This phase has not been observed in this study by SEM and is hardly detectable with X-ray diffraction. When niobium content increased further, the microhardness gradually decreased.

4. Conclusion

The results of this work show the similarities of mechanical and microstructural properties between parts manufactured using pre-alloyed powder and differential injection. Moreover, the homogeneous distribution of the chemical composition in the deposited material using differential injection was validated, thus confirming the ability of the DED-CLAD® process to manufacture *in situ* parts.

In addition, this study presented the advantages of differential injection in manufacturing specific binary or multi-component alloys and offers a solution to fill the gap left by the lack of specific alloys that are not commercially available. Several conclusions can be drawn on the functionally graded parts manufactured in this study. The functionally graded Ti-Nb samples, with several incremental increases of Nb content, were successfully manufactured using the DED-CLAD® process. The homogeneous distribution of the mixture has been validated by X-ray tomography and chemical analyses. Unmelted Nb particles have been identified and localised at the interfaces between layers. The quantification performed by optical microscopy indicated the presence of a maximum of 4% of unmelted particles, which could be reduced by increasing the density energy, as suggested by some authors. Mechanical tests showed a decrease of the microhardness with the increase of Nb content. The elastic modulus was found to be lowest for Ti-

40Nb, which explains the interest of these alloys for biomedical applications.

Further work is currently focused on understanding the presence of unmelted particles in the Ti-Nb deposition while unmelted particles were not observed in the full niobium deposition.

Acknowledgments

The authors acknowledge H.C. Starck Tantalum and Niobium GmbH, powder manufacturer, for providing the pre-alloyed Ti44Nb powder; Patrick MOLL; Julien GUYON; Amélie THIRIET; Robert ALLEN; Eric FLEURY; Grégoire CHABROL; Yannick LAFUE.

References

Abioye, T.E., Farayibi, P.K., Kinnel, P., Clare, A.T., 2015. Functionally graded Ni-Ti microstructures synthesised in process by direct laser metal deposition. Int. J. Adv. Manuf. Technol. 79, 843–850.

Bandyopadhyay, A., Krishna, B.V., Xue, W., Bose, S., 2009. Application of Laser Engineered Net shaping (LENS) to manufacture porous and functionally graded structures for load bearing implants. J. Mater. Sci. Mater. Med. 20, 29–34.

Carroll, B.E., Otis, R.A., Borgonia, J.P., Suh, J., Dillon, R.P., Shapiro, A.A., Hofmann, D.C., Liu, Z.-K., Beese, A.M., 2016. Functionally graded material of 304L stainless steel and inconel 625 fabricated by directed energy deposition: characterization and thermodynamic modeling. Acta Mater. 108, 46–54.

Cheung, C., 2015. Characterization of laser deposited Ti-6Al-4V to Nb gradient alloys. Senior Project Report.

Chlebus, E., Kuznicka, B., Kurzynowski, T., Dybala, B., 2011. Microstructure and mechanical behaviour of Ti-6Al-7Nb alloy produced by selective laser melting. Mater. Charact. 62, 488–495.

Chlebus, E., Kuznicka, B., Dziedzic, R., Kurzynowski, T., 2014. Titanium alloyed with rhenium by selective laser melting. Mater. Sci. Eng. A 620, 155–163.

Collins, P.C., Banerjee, R., Banerjee, S., Fraser, H.L., 2003. Laser deposition of compositionally graded titanium–vanadium and titanium–molybdenum alloys. Mater. Sci. Eng. A 352, 118–128.

DebRoy, T., Basu, S., Mundra, K., 1991. Probing laser induced metal vaporization by gas dynamics and liquid pool transport phenomena. J. Appl. Phys. 70, 1313–1319.

Domack, M.S., Baughman, J.M., 2005. Development of nickel-titanium graded composition components. Rapid Prototyp. J. 11, 41–51.

Elmay, W., Prima, F., Gloriant, T., Bolle, B., Patoor, E., Laheurte, P., 2013. Effect of thermomechanical process on the microstructure and mechanical properties of fully martensitic titanium-based medical alloy. J. Mech. Behav. Biomed. Mater. 18, 47–56.

Fallah, V., Corbin, S.F., Khajepour, A., 2010. Solidification behaviour and phase formation during pre-placed laser cladding of Ti45Nb on mild steel. Surf. Coat. Technol. 204, 2400–2409.

Farayibi, P.K., Folkes, J.A., Clare, A.T., 2013. Laser deposition of Ti-6Al-4V wire with WC powder for functionally graded components. Mater. Manuf. Process. 28, 514–518.

Fischer, M., Joguet, D., Robin, G., Peltier, L., Laheurte, P., 2016. In situ elaboration of a binary Ti-26Nb alloys by selective laser melting of element titanium and niobiom mixed powders. Mater. Sci. Eng. C 62, 852–859.

Fischer, M., Laheurte, P., Acquier, P., Joguet, D., Peltier, L., Petithory, T., Anselme, K., Mille, P., 2017. Synthesis and characterization of Ti-27.5Nb alloy made by CLAD® additive manufacturing process for biomedical applications. Mater. Sci. Eng. C 75, 341–348.

Germain, L., Gey, N., Mercier, R., Blaineau, P., Humbert, M., 2012. An advanced approach to reconstructing parent orientation maps in the case of approximate orientation relations: application to steels. Acta Mater. 60, 4551–4562.

Greses, J., Hilton, P.A., Barlow, C.Y., Steen, W.M., 2004. Plume attenuation under high power Nd:yttritium–aluminum–garnet laser welding. J. Laser Appl. 16, 9–15.

Han, M.-K., Kim, J.-Y., Hwang, M.-J., Song, H.-J., Park, Y.-J., 2015. Effect of Nb on the microstructure, mechanical properties, corrosion behavior, and cytotoxicity of Ti-Nb alloys. Materials 8, 5986–6003.

Ho, W.F., Ju, C.P., Chern Lin, J.H., 1999. Structure and properties of cast binary TiMo alloys. Biomaterial 20, 2115–2122.

Hofmann, D.C., Roberts, S., Otis, R., Kolodziejska, J., Dillon, R.P., Suh, J., Shapiro, A.A., Liu, Z.-K., Borgonia, J.-P., 2014. Developing gradient metal alloys through radial deposition additive manufacturing. Sci. Rep. 4, 1–8.

Kim, H.Y., Satoru, H., Kim, J.I., Hosoda, H., Miyazaki, S., 2004. Mechanical properties and shape memory behavior of Ti-Nb alloys. Mater. Trans. 45, 2443–2448.

Kim, J.I., Kim, H.Y., Hosoda, H., Miyazaki, S., 2005. Shape memory behavior of Ti-22Nb-(0.5-2.0)O(at%) biomedical alloys. Mater. Trans. 46, 852–857.

Kottcamp, E.H., Langer, E.L., 1992. Alloy Phase Diagrams.

Lee, C.M., Ju, C.P., Chern Lin, J.H., 2002. Structure-property relashionship of cast Ti-Nb alloys. J. Oral Rehabil. 29, 314–322.

Mahamood, R.M., Akinlabi, E.T., 2015. Laser metal deposition of functionally graded Ti6Al4V/TiC. Mater. Des. 84, 402–410.

Matsunawa, A., Ohnawa, T., 1991. Beam-plume interaction in laser materials processing. Trans. JWRI 20, 9–15.

Nag, S., Banerjee, R., Fraser, H., 2007. A novel combinatorial approach for understanding microstructural evolution and its relationship to mechanical properties in metallic biomaterials☆. Acta Biomater. 3, 369–376.

Pulugurtha, S.R., 2014. Functionally Graded Ti6Sl4V and Inconel 625 by Laser Metal Deposition.

Qian, X., Dutta, D., 2003. Design of heterogeneous turbine blade. Comput. Aided Des. 35, 319–329.

Schneider-Maunoury, C., Weiss, L., Acquier, P., Boisselier, D., Laheurte, P., 2017. Functionally graded Ti6Al4V-Mo alloy manufactured with DED-CLAD ® process. Addit. Manuf. 17, 55–66.

Schwab, H., Prashanth, K., Löber, L., Kühn, U., Eckert, J., 2015. Selective laser melting of Ti-45Nb alloy. Metals 5, 686–694.

Syre, R., 1976. Niobium, Technique de l'ingénieur, m553 (french report).

Thoemmes, A., Bataev, I.A., Belousova, N.S., Lazurenko, D.V., 2016. Microstructure and mechanical properties of binary Ti-Nb alloys for application in medecine. New Mater. Technol. 26–29.

Wang, Q., Han, C., Choma, T., Wei, Q., Yan, C., Song, B., Shi, Y., 2017. Effect of Nb content on microstructure, property and in vitro apatite-forming capability of Ti-Nb alloys fabricated via selective laser melting. Mater. Des. 126, 268–277.

Watari, F., Yokoyama, A., Saso, F., Uo, M., Kawasaki, T., 1997. Fabrication and properties of functionally graded dental implant. Compos. Part B Eng. 5–11.

Wei, Q., Wang, L., Fu, Y., Qin, J., Lu, W., Zhang, D., 2011. Influence of oxygen content on microstructure and mechanical properties of Ti-Nb-Ta-Zr alloy. Mater. Des. 32, 2934–2939.

Weiss, L., Acquier, P., Germain, L., Fleury, E., 2016. Microtexture of Ti6Al4V obtained by direct energy deposition (DED) process. Proc. 13th World Conf. Titan. pp. 1305–1310.

Yao, Q., Sun, J., Xing, H., Guo, W.-Y., 2007. Influence of Nb and Mo contents on phase stability and elastic property of beta-type Ti-X alloys. Trans. Nonferrous Met. Soc. China 17, 1417–1421.

Zhang, W., Liu, Y., Wu, H., Song, M., Zhang, T., Lan, X., Yao, T., 2015. Elastic modulus of phases in Ti–Mo alloys. Mater. Charact. 106, 302–307.